HHS Public Access

Author manuscript

J Vasc Surg. Author manuscript; available in PMC 2018 June 01.

Published in final edited form as:

J Vasc Surg. 2017 June ; 65(6): 1653–1663. doi:10.1016/j.jvs.2016.12.105.

Non-invasive characterization of Carotid Plaque Strain

Amir A. Khan, PhD[1,6], **Siddhartha Sikdar, PhD**[1], **Thomas Hatsukami, MD**[2], **Juan Cebral, PhD**[1], **Michael Jones, MD**[3], **John Huston, MD**[4], **George Howard, DrPh**[5], and **Brajesh K. Lal, MD**[6]

[1]Department of Bioengineering, George Mason University, Fairfax, VA, USA

[2]Department of Surgery, University of Washington, Seattle, WA, USA

[3]Department of Cardiology, Baptist Health Lexington, Lexington, KY, USA

[4]Department of Radiology, Mayo Clinic, Rochester, MN, USA

[5]Department of Biostatistics, UAB School of Public Health, Birmingham, AL, USA

[6]Center for Vascular Diagnostics, Division of Vascular Surgery, University of Maryland School of Medicine, Baltimore, MD, USA

Abstract

OBJECTIVES—Current risk-stratification of internal carotid artery plaques based on diameter-reducing percent stenosis may be unreliable since ischemic stroke results from plaque disruption with atheroembolization. Biomechanical forces acting on the plaque may render it vulnerable to rupture. The feasibility of ultrasound-based quantification of plaque displacement and strain induced by hemodynamic forces, and their relationship to high-risk plaques has not been determined. We studied the feasibility and reliability of carotid plaque strain measurement from clinical B-mode ultrasound images, and the relationship of strain to high-risk plaque morphology.

METHODS—We analyzed carotid ultrasound B-mode cine-loops obtained in patients with asymptomatic ≥50% stenosis during routine clinical scanning. Optical-flow methods were used to quantify plaque-motion and shear-strain during the cardiac-cycle. The magnitude (Maximum Absolute Shear-Strain Rate, MASSR), and variability (information Entropy of Shear-Strain Rate, ESSR and the Variance of Shear-Strain Rate, VSSR) of strain were combined into a composite Shear-Strain-Index (SSI) which was assessed for inter-scan repeatability and correlated with plaque echolucency.

RESULTS—Nineteen patients (mean age 70-years) constituting 36 plaques underwent imaging. 37% (n=7) of patients showed high strain (SSI ≥0.5, and mean MASSR 2.2, ESSR 39.7, VSSR 0.03) in their plaques, while the remaining clustered into a low-strain group (SSI <0.5, MASSR 0.58, ESSR 21.2, VSSR 0.002). The area of echolucent morphology was greater in high-strain

Address for Correspondence: Brajesh K Lal, MD, 22 South Green Street, S10-B00, Baltimore, MD 21201, blal@smail.umaryland.edu, Tel: 410 328 5840, Fax: 410 328 0717.

plaques versus low-strain plaques (28% versus 17%, P=.018). Strain measurements showed low variability on Bland-Altman plots with cluster-assignment agreement of 76% on repeat scanning. Two patients developed a stroke over 2 years of follow-up; both demonstrated high SSI (≥0.5) at baseline.

CONCLUSIONS—Carotid plaque strain is reliably computed from routine B-mode imaging using clinical ultrasound machines. High plaque strain correlates with known high-risk echolucent morphology. Strain measurement can complement identification of patients at high risk for plaque disruption and stroke.

INTRODUCTION

The primary contributor in the pathogenesis of stroke from carotid atherosclerotic stenosis is plaque disruption, rather than hemodynamic compromise from luminal narrowing[1]. The mechanisms for plaque disruption have yet to be determined. While the degree of diameter-reducing stenosis in the internal carotid artery is the standard approach for risk-stratification, two randomized trials have failed to show a relationship between percent stenosis in asymptomatic patients and subsequent stroke[2,3]. A small proportion of asymptomatic patients, however, do harbor plaques that progress to disruption. Selective revascularization of patients with such vulnerable plaques would prevent strokes if they could be identified with clinically available technology. Conversely, unnecessary procedures would be avoided in patients with low-risk plaques.

American Heart Association (AHA) Type VI plaques with enlarging lipid rich necrotic cores, intraplaque hemorrhage and fibrous cap thinning, may lead to disruption and atheroembolization[4–6]. Although approximately 50% of asymptomatic patients with a stenosis harbor plaques with vulnerable morphology, only about 2% of asymptomatic patients develop a stroke at 1 year[2,3,7]. Therefore, morphology alone has limited ability to predict stroke. Plaques undergoing increased deformation or strain during the cardiac cycle are thought to be more susceptible to rupture[8]. Strain depends not only on biomechanical forces but plaque material properties also; such that “softer” plaques may deform more to similar forces. Therefore, disruption could be influenced by biomechanical forces acting on plaques with high-risk morphology and measurement of strain considers both these factors[9]. Validation of this hypothesis requires the development of plaque strain measures that can be employed in large longitudinal studies.

Carotid plaque strain measurements can be obtained using radiofrequency (RF) ultrasound and speckle tracking, though clinical translation is limited by a lack of access to RF data in commercial ultrasound machines[10–12]. B-mode ultrasound imaging is a practical solution for real-time longitudinal evaluation of plaque deformation and strain, but it has not been tested for feasibility or reliability. Moreover, hypoechoic plaques are a morphologic marker for high risk of stroke, however, there is limited information on the relationship between B-mode strain measurements and ultrasound-derived plaque severity indices such as percent stenosis, peak systolic velocity and echogenicity[13,14].

In this study we 1) tested the feasibility of measuring carotid plaque strain from B-mode ultrasound imaging in a clinical vascular laboratory during a routine clinical examination, 2)

assessed whether strain measurements allow reliable separation into low-strain and high-strain plaques, 3) correlated strain with known plaque severity indices and 4) quantified the reliability of our strain indices.

METHODS

Patients

After approval from the University of Maryland Institutional Review Board and signed informed consent, we enrolled 19 asymptomatic adults with ≥50% carotid stenosis without a prior stroke or transient ischemic attack. Demographics and risk factors (hypertension, diabetes mellitus, dyslipidemia, smoking, and coronary artery disease) were recorded. Patients underwent ultrasound imaging at baseline, were managed with optimal medical treatment, and followed with annual clinical examinations for two years[15].

B-mode ultrasound imaging

A clinical ultrasound machine (Ultrasonix SonixTouch, Richmond, BC, Canada) was used with a standard L9-4/38 linear probe. Doppler velocities with consensus velocity criteria were used to estimate the degree of stenosis[16]. B-mode imaging was used to locate the carotid plaque and acquire cine-loops over 3–5 cardiac cycles with breath-holding, in an operator-selected optimal longitudinal orientation demonstrating the plaque at its thickest. The frame-rates and depth settings were selected by the three participating sonographers as appropriate, and varied across patients (10 to 30 frames per second and 3.5 to 4.5 cm, respectively). For each patient, two scans were obtained by the same sonographer with a 1-hour interval, and used to assess reproducibility and intra-observer variability. The initial sequence was not utilized as a guide to co-register the second scan. Sonographers were not aware that the images would be used to compute plaque strain or intra-observer reproducibility. Since images were acquired as part of routine scanning, and not specifically tailored for optimal strain imaging, these data provide an opportunity to gauge the robustness of strain measurement in a clinical environment. The B-mode images were normalized using the procedure outlined by Nicolaides *et al*[17].

Strain Field Estimation

We employed dense optical flow-based speckle tracking for estimation of plaque displacement fields with high spatial resolution[18]. This allowed evaluation of heterogeneity in plaque motion. We measured the axial, lateral and shear strain fields since plaque movement can occur in all planes. Strain was analyzed at peak-systole to identify effects of the largest hemodynamic forces on the plaque (Figure 1), with respect to baseline displacement at end-diastole which was insignificant[19]. The peak-systolic frame in each study was identified using M-mode images derived from the cine-loops using post-processing. Plaque regions in the far and near walls of each image frame were manually outlined[20]. For each patient, a number of distinct plaque regions could be identified on an image sequence. Two plaque regions were considered distinct if (a) they were located on the near and far arterial walls or (b) the plaques were on the same arterial wall but separated by at least 5 mm. Plaques appearing discontinuous due to shadowing were considered a single region, and pixels in the shadow area were excluded for strain analysis. Figure 2 (A) depicts

two outlined plaque regions (blue and red lines) located in the near and far walls respectively. Figure 2 (B) shows a plaque region in the far wall of another patient with significant shadowing. The shear strain fields for each plaque region were analyzed separately.

Computation of Shear Strain Rate and Associated Parameters

The shear strain field for each B-mode cine-loop sequence was normalized by its frame-rate to obtain the shear strain rate field. We computed three parameters to assess the global behavior of the plaque. 1) Maximum Absolute Shear Strain Rate (MASSR), a measure of the magnitude of strain regardless of direction[12]. We introduced two measures for the spread or variability in magnitude or direction of the strain fields within the plaque: 2) Variance of Shear Strain Rate (VSSR) specifies the dispersion of strain and 3) Entropy of Shear Strain Rate (ESSR) measures the discordance within the plaque tissue. While MASSR could have been used as the only feature for measuring strain, the addition of the other two features make the strain measurement more robust. This advantage is highlighted in the results section during cluster assignment for the repeat scans. These three-dimensional strain features (MASSR, VSSR and ESSR) for each plaque provide a complete picture of plaque dynamics and we combined them for each plaque region "*i*" after normalization, to obtain a normalized shear strain rate ($NSSR_i$):

$$\mathrm{NSSRI}_i = \frac{1}{3}\left(\frac{\mathrm{MASSR}-\mu_{\mathrm{MASSR}}}{\sigma_{\mathrm{MASSR}}}+\frac{\mathrm{VSSR}-\mu_{\mathrm{VSSR}}}{\sigma_{\mathrm{VSSR}}}+\frac{\mathrm{ESSR}-\mu_{\mathrm{ESSR}}}{\sigma_{\mathrm{ESSR}}}\right),$$

where, (μ_{MASSR}, μ_{VSSR}, μ_{ESSR}) and (σ_{MASSR}, σ_{VSSR}, σ_{ESSR}) correspond to the means and standard deviations of the respective strain parameters for 36 plaque regions in 19 patients.

Shear Strain Index-Logistic Regression

To investigate the distribution of plaque strains, NSSRs from the 36 plaque regions were clustered using a *2*-class *k*-means classifier. The classifier computes one centroid per cluster and assigns a plaque region to one of the two clusters based on minimal distance from the centroids. The resulting two clusters separate plaques with predominantly low NSSR (low-strain) from those with predominantly high NSSR (high-strain). This allows evaluation of the prevalence of low-strain versus high-strain plaques. We tested the reliability of our cluster-assignment using a silhouette plot, which indicates the score (−1 to +1) for attribution of each plaque to its respective cluster. Positive and higher average values for a cluster indicate a stronger association.

We then computed a shear strain index (SSI) using logistic regression (LR). The LR model computed the logistic function representing the probability of association to a particular cluster and was considered the SSI for a particular plaque. Since SSI represented probability, a threshold of 0.5 was set to assign the plaque as high-strain or low-strain. When a new test-plaque "*t*" was evaluated, its normalized shear strain rate $NSSR_t$ was computed, and then the SSI was computed as: $\mathrm{SSI}_t == \frac{1}{1+e^{-(\theta_0+\theta_1\mathrm{NSSR}_t)}}$, where θ_0 and θ_1 are LR-model coefficients. This SSI value gives a probabilistic estimate of the likelihood of the plaque

being high-strain. The decision on this plaque "t" being high-strain or low-strain was then taken as:

$$\begin{aligned} &\text{Low}-\text{strain:SSI}_t < 0.5, \\ &\text{High}-\text{strain:SSI}_t \geq 0.5 \end{aligned}$$

Shear Strain Index Repeatability

The repeatability of the proposed comprehensive strain measure (SSI) was established by an inter-scan analysis using a repeat B-mode cine-loop. As with the first (index) scan, each plaque region was analyzed and assigned to one of two clusters, depending on its SSI value. The SSI for the repeat scan was independent of that from the first scan since analyses were performed after both scans were completed and sonographers were blinded to the results of the analyses.

Characterization of plaque morphologic features

Pixel brightness intensities were measured for each outlined plaque region to differentiate plaque tissue characteristics[21]. The area of regions with a brightness intensity <25 were measured to compute the percentage of plaque region that was echolucent[22]. The Doppler peak systolic velocity (PSV) was measured at the region of maximal stenosis with the transducer held at a 60-degree angle. The percent echolucent region, PSV and velocity-derived percent stenosis were correlated with SSI.

Statistical Analysis

Statistical analysis was performed in MATLAB (Mathworks, Natick, MA). Strain rates are presented in units of 1/second. Continuous data are presented as median±standard deviation (SD). Significance levels were set to 95% confidence intervals with $P<.05$ considered significant. Pearson's correlation coefficient (r) was used to assess the relationship of plaque shear strain parameters to echolucency. The inter-scan reliability of cluster-assignment was measured using the proportion of plaque regions assigned to the same cluster for both scan sequences, and displayed by Bland-Altman plots, Inter Class Correlation (ICC), Minimum Detectable Change (MDC) and bias in the inter-scan strain features. The MDC was computed at 95% confidence interval as: $\text{MDC}=1.96\sqrt{2}\text{SEM}$, where SEM is the standard error of measurement, $\text{SEM}=SD\sqrt{1-\text{ICC}}$. Bias indicates the mean difference (θ) in Bland-Altman plots.

RESULTS

Full field strain rates

Demographic features and vascular risk-factors for our patients are described in Table I. All patients were included in the analysis regardless of their image quality, to assess the performance of the proposed strain measures in a realistic clinical set-up. The application of dense optical flow scheme to successive B-mode image-pairs resulted in axial and lateral displacement fields where the lateral component was depicted along the x-axis (scan-line) and the axial component along the y-axis (depth). Figure 3 (A) shows the displacement

fields for the two plaque regions of Figure 2 (A). Figure 3 (B) presents displacement for the plaque in Figure 2 (B) and it exhibits more pronounced displacement as highlighted by the magnitude of the displacement vectors. The quiver-plots in Figure 3 (C)–(D) display the combined lateral and axial displacements in the plaque regions at peak-systole. The strains estimated from these inter-frame displacements were normalized by their respective frame-rates to obtain the axial, lateral and shear strain rates. The strain rates for the two patients in Figure 2 (A) and (B) are shown in Figure 4. Plaque strain did not manifest significant differences along the axial direction (Figure 4 (C)–(D)) with both patients exhibiting similar strains. Plaques exhibited more significant dynamic patterns in the lateral direction (Figure 4 (E)–(F)). The shear strain rate plots in Figure 4 (A)–(B) show that both plaque regions in the first patient (from Figure 2 (A)) exhibit smaller and uniform strain throughout the plaque whereas the distribution in the second patient (from Figure 2 (B)) is non-uniform with higher strain rates in certain regions. We computed shear strain rates in a similar fashion for all plaques in each patient.

Shear strain rate-based plaque assessment

2D scatterplots of the strain rate features (ESSR, MASSR and VSSR) for the 36 plaque regions are shown in Figures 5 (A)–(C). Normalized shear strain rates (NSSRs) in these plaque regions were clustered using the binary *k*-means classifier (Figure 5 (D)). The silhouette plot of the classification (Figure 5 (E)) indicates good clustering, with higher variability in the high-strain plaques. A logistic regression model was developed to compute the Shear Strain Index (SSI, Figure 5 (F)) for each plaque, whereas patient-wise results are shown in Figure 5 (G). The dotted red lines indicate the decision boundary of 0.5. The associated strain features of MASSR, ESSR and VSSR were also evaluated for their consistency. The respective correlations between the features: MASSR/VSSR: .90; MASSR/ESSR: .72; ESSR/VSSR: .64 ($P < .001$) indicate that all the measures are concordant yet unique. There was a significant difference between the median NSSRs of the two clusters (178%, $P < .001$). For patients with multiple plaque regions, if one of their plaque regions exhibited high strain, the patient was assigned a high-strain category. Three of the 19 patients had both high-strain and low-strain plaque regions. Among the 11 patients who had two or more plaques, the SSI correlation between plaques for the same patient was .46 ($P=.17$), with the average parameter variabilities of: SSI (0.12), MASSR (0.35), ESSR (8.45) and VSSR (0.005). Results of both per-plaque region and per-patient analyses are presented in Table II. In our cohort, 37% of patients (n= 7) were attributed to the high-strain cluster. A very high cluster attribution conformity was obtained between the patient-wise and plaque-wise results (correlation of .86, $P<<.01$). Results for the 19 plaque regions in the regions of highest stenosis indicated that 6 plaque regions exhibited high strain.

Correlation of strain parameters to plaque echolucency

Plaque echolucency was used as an indicator for the presence of lipid-rich necrotic core content. It was measured from the longitudinal B-mode images using the percentage of plaque area with pixel brightness <25. The Shear Strain Index correlated with plaque echolucency (+0.47, P < .002). The individual shear strain features also correlated with echolucency: MASSR (+0.58), VSSR (+0.43) and ESSR (+0.40). Figure 6 is a box-whisker plot, demonstrating the proportion of echolucent segments in plaques assigned to low-strain

and high-strain clusters. The median echolucent area for high-strain plaques (median 28%, n = 14) was 61% higher than that for low-strain plaques (median 17%, n = 22). The two-sample t-test revealed significant difference between the two classes (P=.18). The variability indices were: low-strain (SD=11.28, 25th percentile:9.4, 75th percentile:24.6) and high-strain low-strain (SD=17.6, 25th percentile:9.4, 75th percentile:45.2).

Relationship of strain parameters to PSV and stenosis

Since percent stenosis is currently used for assessment of plaque severity and for risk-stratification, results of strain-based clustering were assessed against percent stenosis and PSV. Three of the 19 patients had ≥70% stenosis, all of whom were assigned to the high-strain cluster. The other 5 patients in the high-strain cluster had 50–69% stenosis. The PSV values correlated with SSI (0.51, P < .03), though the median PSV value for high-strain plaques (180 cm/s) did not differ significantly from low-strain plaques (135 cm/s). Two patients suffered a stroke during follow-up; both patients had plaques that were categorized as high-strain.

Inter-scan repeatabilty of strain indices

The inter-scan repeatability of our strain indices was examined by repeating the measurements on a second scan. Shear Strain Indices (SSI) were computed and cluster-assignment performed on both scans. The cluster assignment repeatability was only 74% when MASSR alone was used. The cluster-assignment repeatability increased to 76% when the SSI was used, despite the fact that image-quality in the repeat scans were not always consistent with the first scan. Bland-Altman plots for the shear strain features, MASSR, ESSR, VSSR, (Figure 7 (A)), NSSRs (Figure 7 (B)) and SSIs (Figure 7 (C)) for the two scans confirmed that most of the values fell within the 95% confidence interval (±1.96 σ). The additional inter-scan reliability statistics were: shear strain features (MDC=3.17, ICC=0.86, SEM=1.15 and bias=−0.09); NSSR (MDC=0.695, ICC=0.55, SEM=0.25 and bias=0.04); and SSI (MDC=0.285, ICC=0.62, SEM=0.1 and bias=0.03).

DISCUSSION

Our study evaluated the feasibility, utility and reliability of measuring carotid plaque strain using B-mode ultrasound image sequences acquired in a clinical vascular laboratory for asymptomatic patients. We found that 1) strain measures separated plaques into distinct low-strain and high-strain clusters, with 37% falling in a high-strain group, 2) high strain measures were found in plaques with more echolucent regions and not always in plaques with a high peak systolic velocity or percent stenosis, 3) our proposed Shear Strain Index (a composite of strain magnitude, direction and spread) can be measured reliably with clinically available vascular ultrasound equipment.

Repetitive deformation of plaques from blood-flow and cardiac cycle-induced motion can result in excessive plaque strain. Acting over time, these forces can induce tissue fatigue which may contribute to plaque disruption. Due to its high temporal resolution, duplex ultrasonography is well-suited for imaging plaque motion, deformation and resulting plaque strain during the cardiac cycle. Studies using radiofrequency (RF) ultrasonography in a

research environment have shown that in symptomatic patients, carotid plaques had asymmetric discordant motion with high strain compared to asymptomatic plaques[11,12]. This approach was used by Huang *et. al.*, who also correlated their findings with magnetic resonance imaging (MRI) morphology[12]. However, clinical vascular laboratories do not have access to machines that record RF data. Our analyses can be performed using RF data if and when they become readily available in clinical machines. We therefore utilized B-mode ultrasound images acquired with clinical machines in a hospital vascular laboratory, and applied standard optical flow-based speckle-tracking techniques to evaluate plaque motion[8,11,12]. Our study demonstrates, for the first time, that carotid plaque strain can be reliably measured in a clinical setting. The images analyzed in this study were collected as part of a clinical evaluation and not as a standardized research protocol. These findings have implications for the translation of strain measurement into clinical practice, and its implementation in large-scale longitudinal clinical studies that accrue patients from multiple clinical centers.

Emerging information indicates that enlarging lipid-rich necrotic cores and intraplaque hemorrhage (IPH) are markers for future stroke. These histo-morphological changes have been observed in surgical carotid plaque specimens from patients with symptomatic (transient ischemic attacks or stroke) carotid disease[1]. Different tissues reflect ultrasound to varying degrees, therefore image-brightness on B-mode imaging has been correlated with plaque tissue composition. Lipid-rich necrotic cores and IPH typically appear as dark or echolucent regions on B-mode images[13,22]. Plaques with large echolucent areas are associated with an increased risk of future stroke[13,14]. The largest study assessing ultrasound-based tissue characterization found that the area occupied by regions with low echogenicity (brightness <25) had a linear association with future stroke. The annual stroke rate was 0.4% when the echolucent area was <4 mm^2 and was 5% for areas >10 mm^2 [22]. In our study, the Shear Strain Index (SSI) of plaques correlated with plaque echolucency, indicating that plaques with higher strain correlated with high-risk morphologic features that are known to be present in symptomatic and unsa plaques. While plaque with high strain correlated with known high-risk morphology, Figure 6 also highlights an overlap between the 25th percentile of one cluster and the 75th percentile of the other. This indicates that both morphology (echolucent regions) and biomechanics (high strain), may impart a certain degree of risk. The total time for acquisition and post-processing of the B-mode cine-loop for strain index computation is about 35 minutes which can be optimized to reduce it even further.

Limitations

First, we did not perform MRI measurement of plaque morphology. However, MRI morphologic assessment has been correlated with RF-based strain measurement[12]. We therefore focused on testing feasibility of translating strain measurement into clinical practice and on identifying the most clinically relevant strain measure. Second, the number of patients in our study was small. Our results, however, confirm the feasibility and reliability of strain measurement in a clinical environment. We consider this an important first step prior to embarking on a planned acquisition of data from a larger cohort in the Carotid Revascularization and Medical Management for Asymptomatic Carotid Stenosis

Trial (CREST-2)[23]. Third, most of the patients in our study-sample were in the 50–69% stenosis range. It is possible that patients in the higher stenosis range could have strengthened the high-strain cluster findings; although, as with plaque echolucency, it is likely that strain measures may work independent of degree of stenosis. Two patients suffered a clinical stroke during the two-year follow-up period, and both had plaques that were categorized to the high-strain cluster based on our proposed strain index. One had a stenosis in the 50–69% range while the other had ≥70% stenosis. Fourth, the inter-scan reproducibility of our proposed strain metric showed reasonable, but not perfect results (76% repeated cluster assignment). This highlights the inherent limitations of B-mode ultrasound imaging which is susceptible to operator-dependence, shadowing and image-quality effects. The current study analyzed all the B-mode scans irrespective of their quality, thereby representing a true sample of clinical studies. Since, B-mode image acquisition is relatively quick, approaches for enhancing the reliability of strain indices may include acquiring multiple scans from a patient and calculating an aggregate strain score; increasing the number of cardiac cycles sampled, and increasing the number of frames per second recorded.

CONCLUSIONS

Carotid plaque shear strain measurements can be computed from B-mode ultrasound imaging during routine clinical vascular examinations using standard ultrasound machines. The measures are reliable and high strain scores correlate with high-risk echolucent plaques. Our proposed Shear Strain Index incorporates the magnitude, direction and dispersion of carotid plaque strain, and may offer a complementary approach to identify patients at high risk for future plaque disruption and stroke. Whether these findings translate into an independent predictor of stroke will need to be evaluated in larger longitudinal studies.

Acknowledgments

John Yokemick RVT, Rachel Butrim RVT and Matthew Startzel RVT for their role in performing duplex ultrasonography for our patients.

References

1. Redgrave JN, Lovett JK, Gallagher PJ, Rothwell PM. Histological assessment of 526 symptomatic carotid plaques in relation to the nature and timing of ischemic symptoms: the Oxford plaque study. Circulation. 2006; 113(19):2320–8. [PubMed: 16651471]
2. Walker MD, Marler JR, Goldstein M, Grady PA, Toole JF, Baker WH, et al. Endarterectomy for asymptomatic carotid artery stenosis. Jama. 1995; 273(18):1421–1428. [PubMed: 7723155]
3. Halliday A, Mansfield A, Marro J, Peto C, Peto R, Potter J, et al. Prevention of disabling and fatal strokes by successful carotid endarterectomy in patients without recent neurological symptoms: randomised controlled trial. Lancet. 2004; 363(9420):1491–1502. [PubMed: 15135594]
4. Carr S, Farb A, Pearce WH, Virmani R, Yao JS. Atherosclerotic plaque rupture in symptomatic carotid artery stenosis. J Vasc Surg. 1996; 23(5):755–766. [PubMed: 8667496]
5. Stary HC. Natural history and histological classification of atherosclerotic lesions an update. Arterioscler Thromb Vasc Biol. 2000; 20(5):1177–1178. [PubMed: 10807728]
6. Fisher M, Paganini-Hill A, Martin A, Cosgrove M, Toole JF, Barnett HJ, et al. Carotid plaque pathology thrombosis, ulceration, and stroke pathogenesis. Stroke. 2005; 36(2):253–257. [PubMed: 15653581]

7. Saam T, Underhill HR, Chu B, Takaya N, Cai J, Polissar NL, et al. Prevalence of American Heart Association type VI carotid atherosclerotic lesions identified by magnetic resonance imaging for different levels of stenosis as measured by duplex ultrasound. J Am Coll Cardiol. 2008 Mar 11; 51(10):1014–21. [PubMed: 18325441]
8. Beaussier H, Naggara O, Calvet D, Joannides R, Guegan-Massardier E, Gerardin E, et al. Mechanical and structural characteristics of carotid plaques by combined analysis with echotracking system and MR imaging. JACC Cardiovasc Imaging. 2011; 4(5):468–477. [PubMed: 21565733]
9. Harloff A. Carotid plaque hemodynamics. Interv Neurol. 2012; 1(1):44–54. [PubMed: 25187766]
10. McCormick M, Varghese T, Wang X, Mitchell C, Kliewer MA, Dempsey RJ. Methods for robust in vivo strain estimation in the carotid artery. Phys Med Biol. 2012; 57(22):7329. [PubMed: 23079725]
11. Widman E, Caidahl K, Heyde B, D'hooge J, Larsson M. Ultrasound speckle tracking strain estimation of in vivo carotid artery plaque with in vitro sonomicrometry validation. Ultrasound Med Biol. 2015; 41(1):77–88. [PubMed: 25308946]
12. Huang C, Pan X, He Q, Huang M, Huang L, Zhao X, et al. Ultrasound-Based Carotid Elastography for Detection of Vulnerable Atherosclerotic Plaques Validated by Magnetic Resonance Imaging. Ultrasound Med Biol. 2016; 42(2):365–377. [PubMed: 26553205]
13. Grønholdt M-LM, Nordestgaard BG, Schroeder TV, Vorstrup S, Sillesen H. Ultrasonic echolucent carotid plaques predict future strokes. Circulation. 2001; 104(1):68–73. [PubMed: 11435340]
14. Gupta A, Kesavabhotla K, Baradaran H, Kamel H, Pandya A, Giambrone AE, et al. Plaque Echolucency and Stroke Risk in Asymptomatic Carotid Stenosis A Systematic Review and Meta-Analysis. Stroke. 2015; 46(1):91–97. [PubMed: 25406150]
15. Ricotta JJ, AbuRahma A, Ascher E, Eskandari M, Faries P, Lal BK. Updated Society for Vascular Surgery guidelines for management of extracranial carotid disease. J Vasc Surg. 2011; 54(3):e1–e31. [PubMed: 21889701]
16. Grant EG, Benson CB, Moneta GL, Alexandrov AV, Baker JD, Bluth EI, et al. Carotid Artery Stenosis: Gray-Scale and Doppler US Diagnosis—Society of Radiologists in Ultrasound Consensus Conference 1. Radiology. 2003; 229(2):340–346. [PubMed: 14500855]
17. Nicolaides AN, Kakkos SK, Griffin M, Sabetai M, Dhanjil S, Thomas DJ, et al. Effect of image normalization on carotid plaque classification and the risk of ipsilateral hemispheric ischemic events: results from the asymptomatic carotid stenosis and risk of stroke study. Vascular. 2005; 13(4):211–221. [PubMed: 16229794]
18. Sun, D., Roth, S., Black, MJ. Computer Vision and Pattern Recognition (CVPR), 2010 IEEE Conference on [Internet]. IEEE; 2010. Secrets of optical flow estimation and their principles; p. 2432-2439.[cited 2016 May 31]Available from: http://ieeexplore.ieee.org/xpls/abs_all.jsp?arnumber=5539939
19. Ku DN, Giddens DP, Zarins CK, Glagov S. Pulsatile flow and atherosclerosis in the human carotid bifurcation. Positive correlation between plaque location and low oscillating shear stress. Arterioscler Thromb Vasc Biol. 1985; 5(3):293–302.
20. AlMuhanna K, Hossain MM, Zhao L, Fischell J, Kowalewski G, Dux M, et al. Carotid plaque morphometric assessment with three-dimensional ultrasound imaging. J Vasc Surg. 2015; 61(3): 690–697. [PubMed: 25499716]
21. Lal BK, Hobson RW, Pappas PJ, Kubicka R, Hameed M, Chakhtura EY, et al. Pixel distribution analysis of B-mode ultrasound scan images predicts histologic features of atherosclerotic carotid plaques. J Vasc Surg. 2002; 35(6):1210–1217. [PubMed: 12042733]
22. Kakkos SK, Griffin MB, Nicolaides AN, Kyriacou E, Sabetai MM, Tegos T, et al. The size of juxtaluminal hypoechoic area in ultrasound images of asymptomatic carotid plaques predicts the occurrence of stroke. J Vasc Surg. 2013; 57(3):609–618. [PubMed: 23337294]
23. Lal BK, Meschia JF, Brott TG. CREST-2: Guiding Treatments for Asymptomatic Carotid Disease (September 2013). Endovasc Today. 2013; 1(9):73–6.

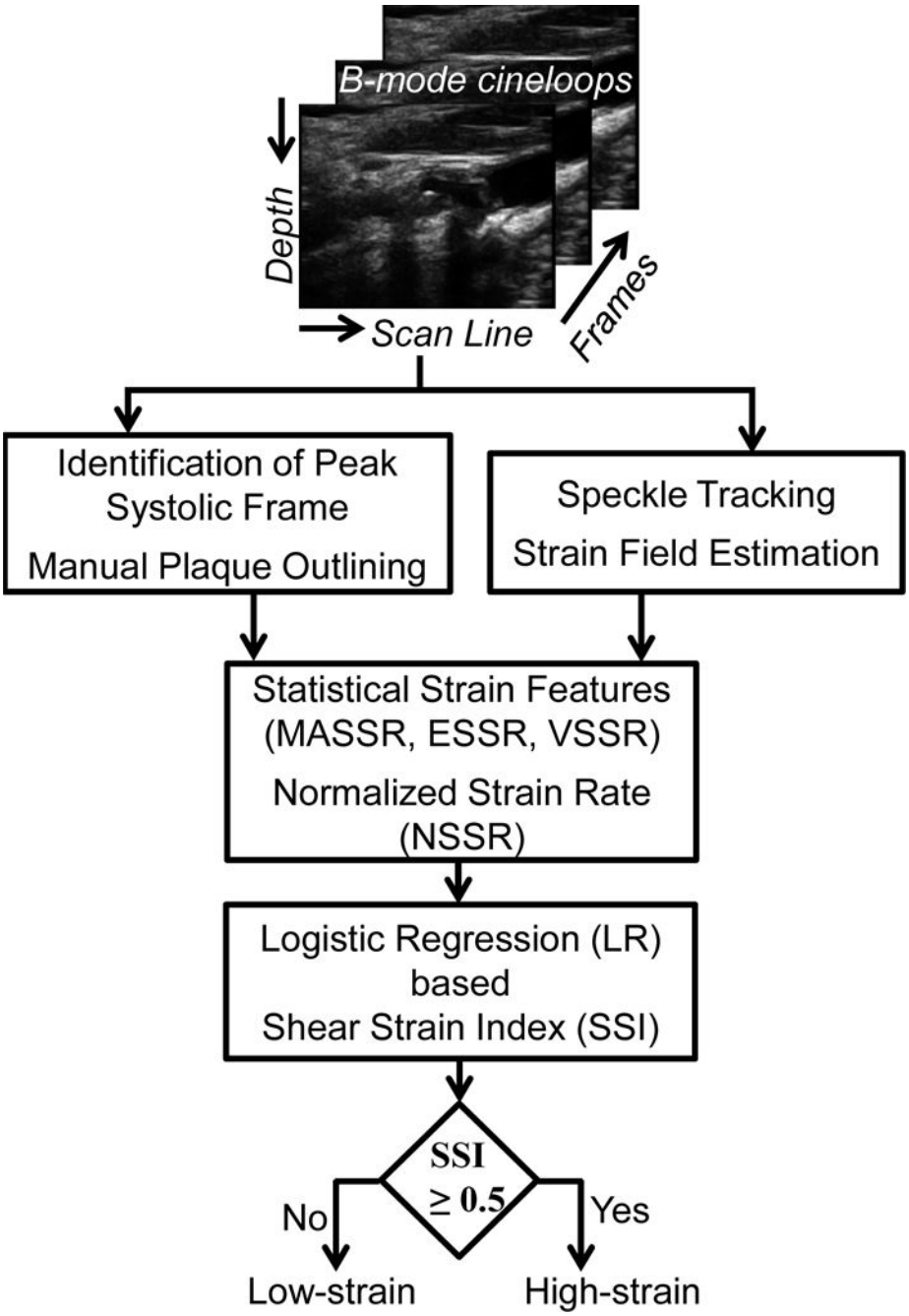

Figure 1.
Process for computing shear strain from B-mode image sequences.

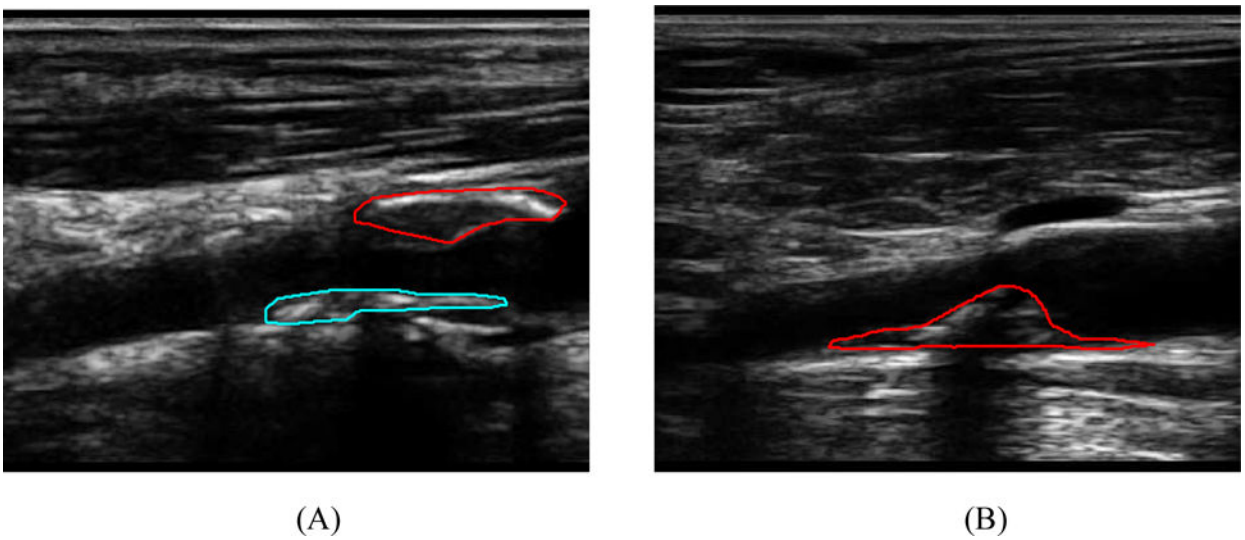

Figure 2.

B-mode images at peak-systole for 2 patients: (a) patient with 2 plaque regions on the near and far arterial walls, (b) patient with a single plaque region on the far wall. Red and blue lines indicate manually outlined plaque regions.

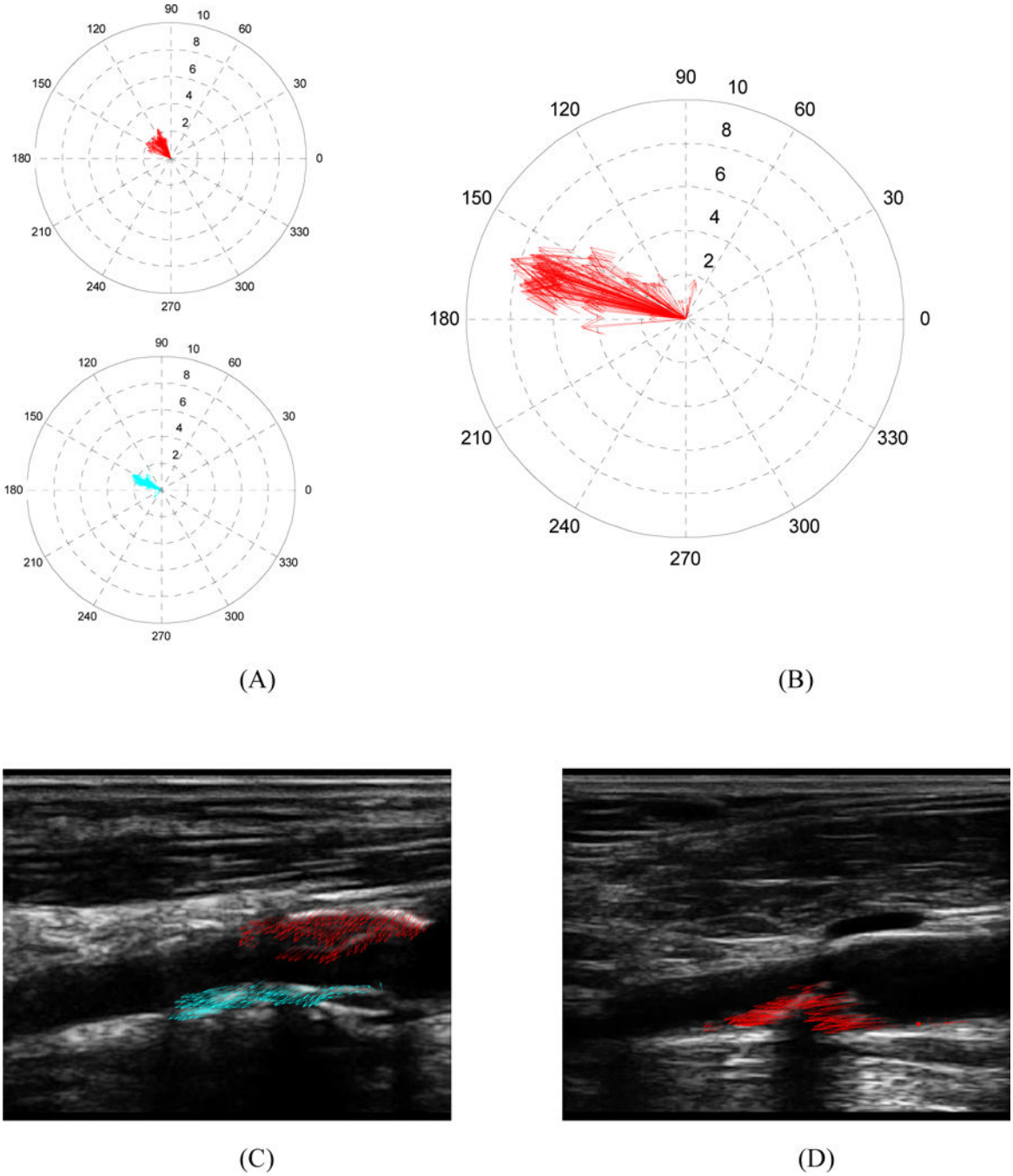

Figure 3.

Speckle tracking-based displacement fields: (a–b) Compass plots representing displacement fields for the plaque regions in (a) the patient of Figure 1 (a), and (b) the patient of Figure 1(b). The length of the arrows represents displacement magnitude and their angle represents angular orientation of displacement. (c–d) Quiver plots showing the displacement vectors superimposed on B-mode images of the plaque regions.

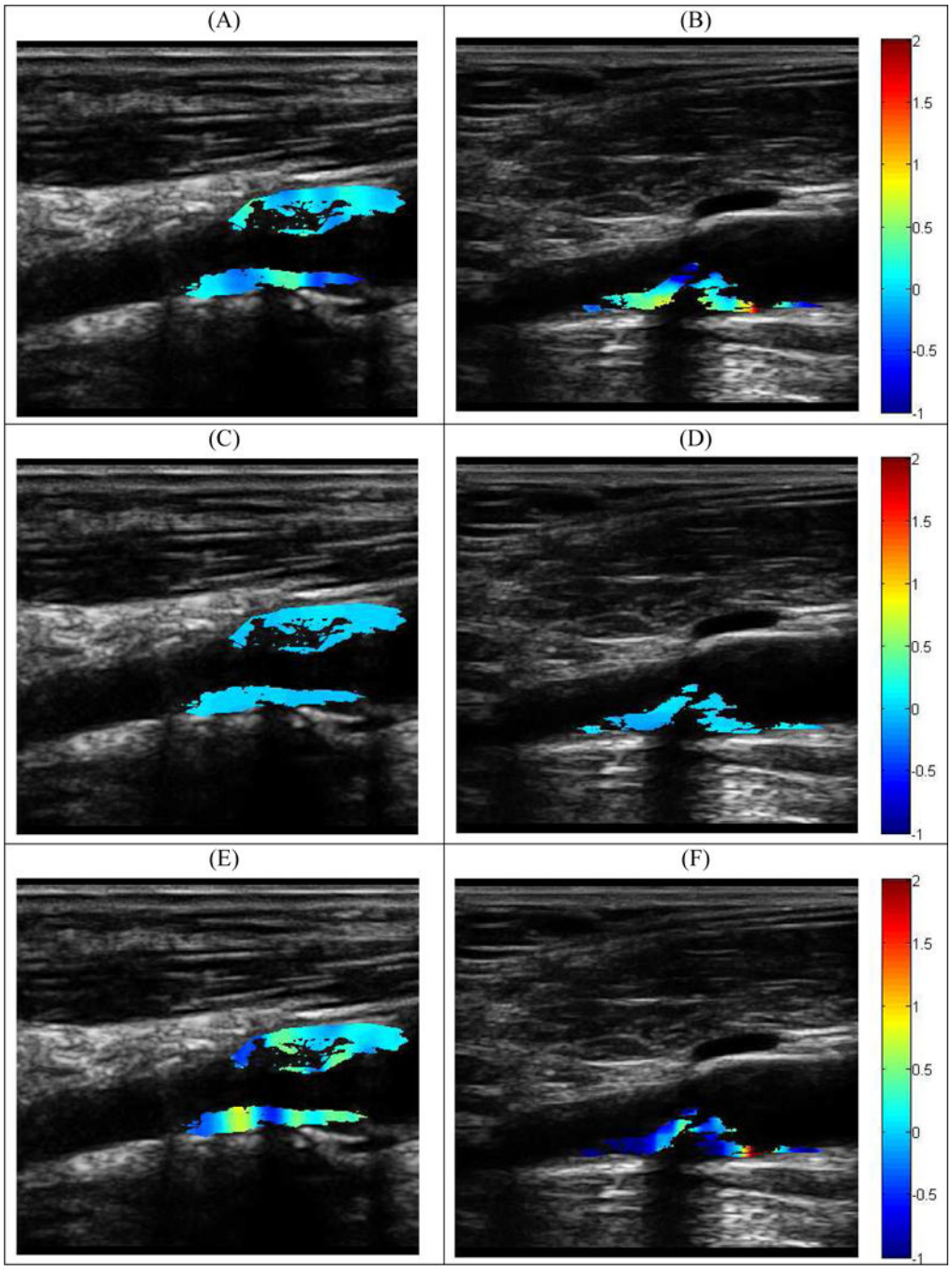

Figure 4.

Instantaneous strain rates for the two patients in Figure 1. (Left) a, c, e correspond to shear, axial and lateral strain rates for the first patient in Figure 1(a). (Right) b, d and f represent similar measurements for the second patient in Figure 1 (b). Colors represent the strain rates.

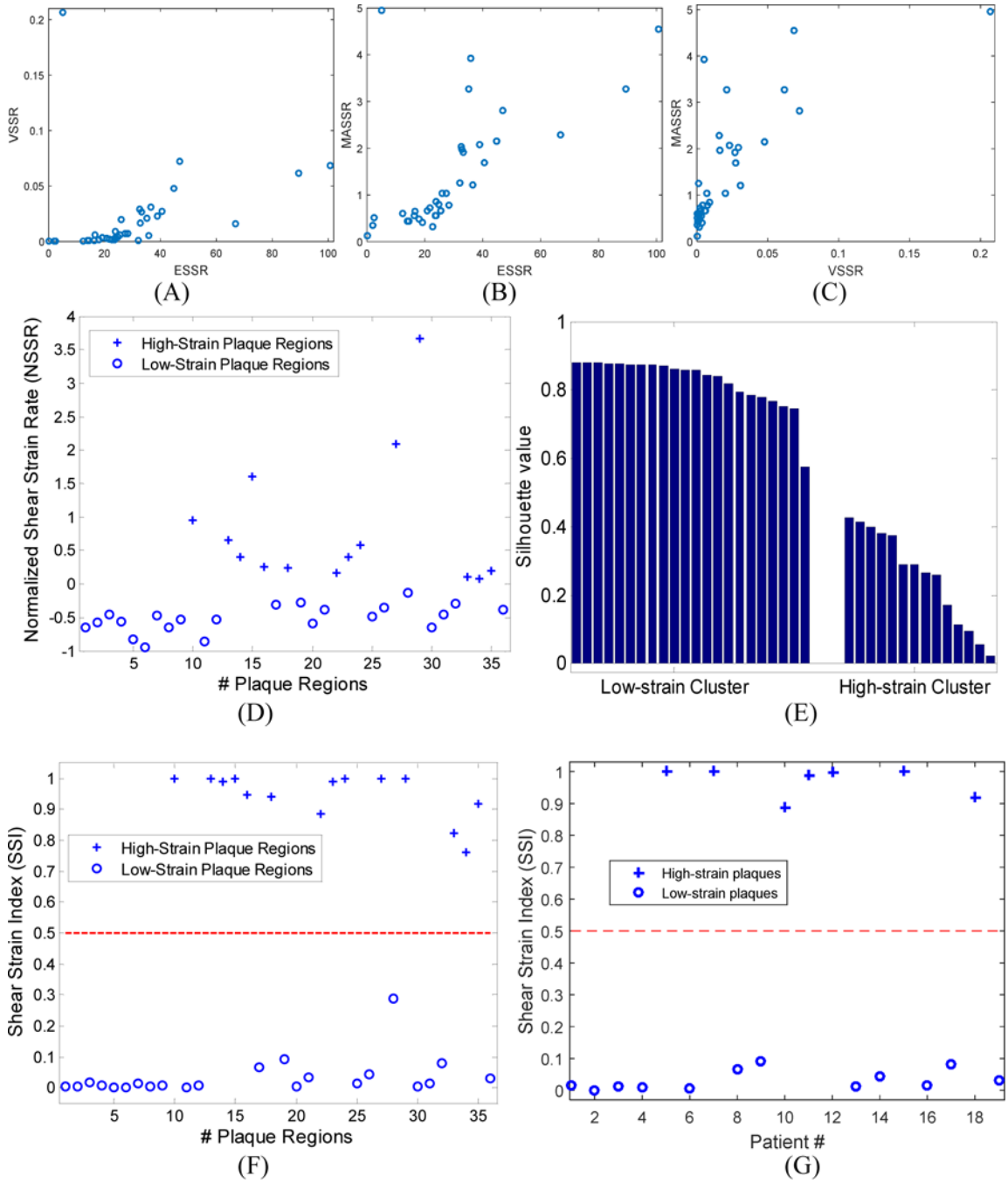

Figure 5.

Cluster-attribution into high or low-strain for 36 plaque regions in 19 patients: (a)–(c) 2D-strain feature scatter plots based on magnitude (Maximum Absolute Shear Strain Rate, MASSR) and spread (Variance Of Shear Strain Rate, VSSR and Entropy Of Shear Strain Rate, ESSR) of strain measurements, (d) Normalized Shear Strain (NSSR) Rate-based *k*-means classification, (e) Silhouette plots indicating the significance of the *k*-means classification shown in (d), (f) Plaque and (g) Patient-wise Shear Strain Indices (SSI) with

the dashed red lines indicating the decision-boundary between high and low strain. ‘+’ and ‘o’ in (d), (f) and (g) indicate high-strain and low-strain cluster-assignments respectively.

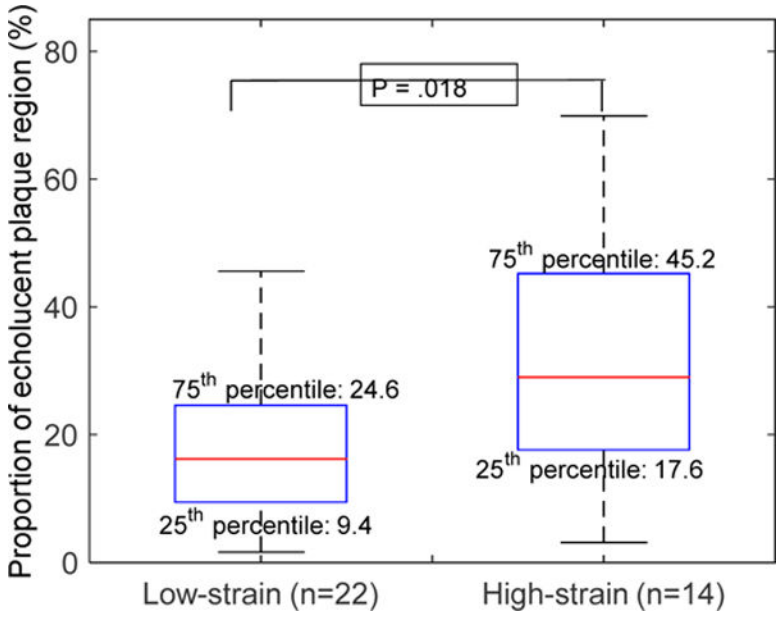

Figure 6.

Box-whisker plot indicating the relationship of plaque echolucency (pixel brightness <25) to strain-based classification for the 36 plaque regions.

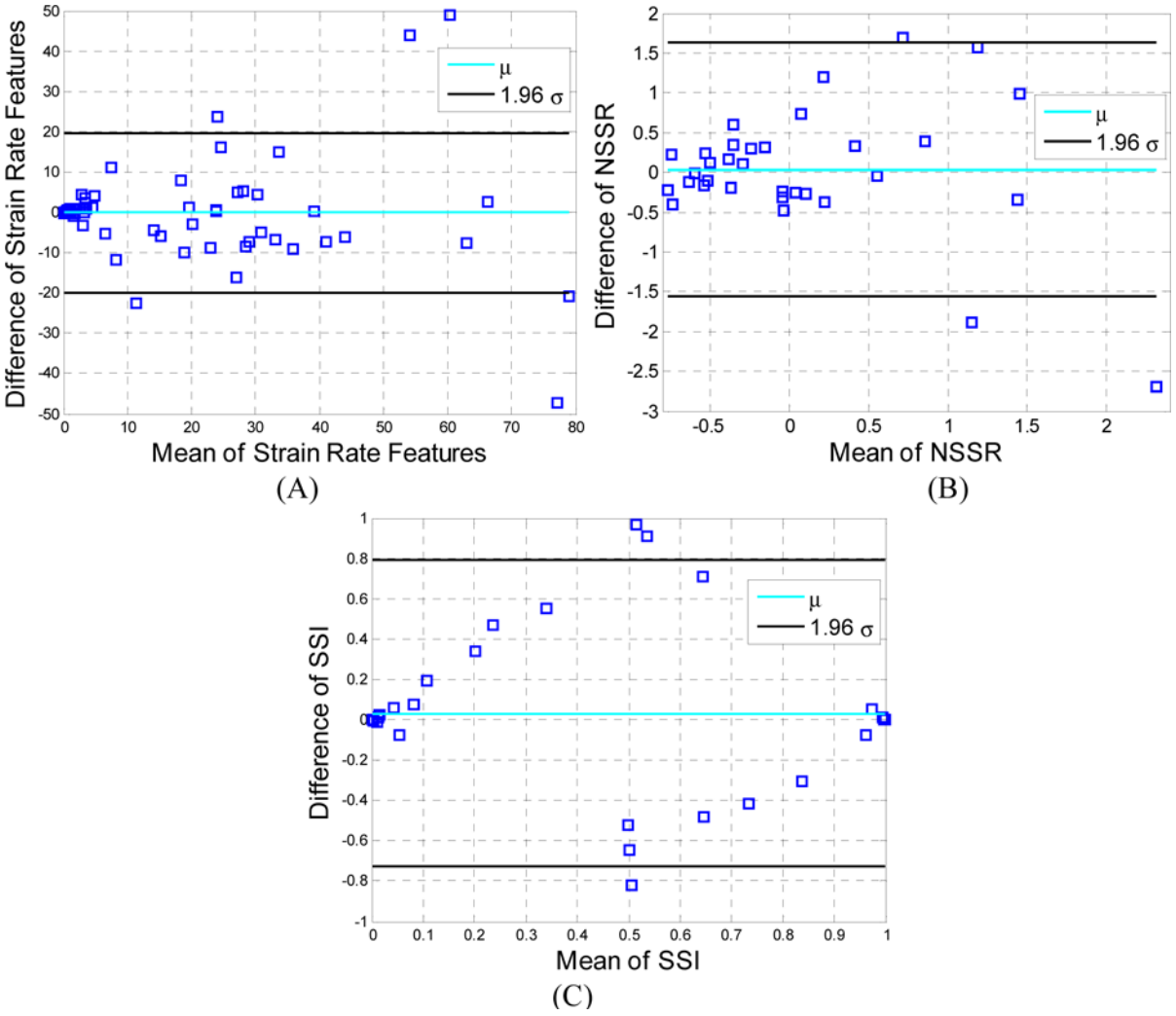

Figure 7.

Bland-Altman plots demonstrating inter-scan variability for the strain metrics: (a) the three 3D strain features: Maximum Absolute Shear Strain Rate (MASSR), Variance Of Shear Strain Rate (VSSR) and Entropy Of Shear Strain Rate (ESSR), (b) Normalized Shear Strain Rate (NSSR), and (c) Shear Strain Index (SSI).

Table I

Demographic and vascular risk-factor information

Variables	***Mean ± SD or Percentage (n = 19)***
Age, years	*70 ± 7*
Male sex	100 (n=19)
Caucasian	79 (n=15)
Diabetes mellitus	47 (n=9)
Coronary artery disease	58 (n=11)
Hypertension	95 (n=18)
Smoking (past or present)	84 (n=16)
Stenosis	
50%–70%	84 (n=16)
≥ 70%	15 (n=3)

SD, Standard deviation

TABLE II

Summary of the shear strain features on 19 patients with 36 plaque regions.

Total patients = 19 Total plaque regions = 36	**Low-strain Cluster**	**High-strain Cluster**
% of patients	63 (n=12)	37 (n=7)
% of plaque regions	61 (n=22)	39 (n=14)
MASSR	0.6 ±0.3	2.2±1.9[a]
ESSR	21±9	40±22[a]
VSSR	0.00±0.00	0.03±.05[a]
NSSR	−0.51±0.20	0.40±1.01[a]
SSI	0.01±0.06	0.98±0.08[a]

MASSR: Maximum Absolute Shear Strain Rate, ESSR: Entropy of Shear Strain Rate; VSSR: Variance of Shear Strain Rate; NSSR: Normalized Shear Strain Rate; SSI: Shear Strain Index;

[a] *P < .0001 compared to the corresponding value in the low-strain cluster.* Correlation between patient-wise and plaque-wise results was .86 (P<. 01).